Biochimica et Biophysica Acta 1798 (2010) 161–166

Contents lists available at ScienceDirect

Biochimica et Biophysica Acta

journal homepage: www.elsevier.com/locate/bbamem

Anesthetic effects on the structure and dynamics of the second transmembrane domains of nAChR α4β2

Tanxing Cui [a,1], Christian G. Canlas [a,1], Yan Xu [a,b], Pei Tang [a,b,c,*]

[a] Department of Anesthesiology, University of Pittsburgh School of Medicine, Pittsburgh, PA 15261
[b] Department of Pharmacology and Chemical Biology, University of Pittsburgh School of Medicine, Pittsburgh, PA 15261
[c] Department of Computational Biology, University of Pittsburgh School of Medicine, Pittsburgh, PA 15261

ARTICLE INFO

Article history:
Received 4 February 2009
Received in revised form 31 July 2009
Accepted 12 August 2009
Available online 26 August 2009

Keywords:
Mechanisms of general anesthesia
Halothane
Isoflurane
Volatile anesthetics
PISEMA
Solid state NMR
nAChR
a4b2
Neuronal nAChR

ABSTRACT

Channel functions of the neuronal α4β2 nicotinic acetylcholine receptor (nAChR), one of the most widely expressed subtypes in the brain, can be inhibited by volatile anesthetics. Our Na^+ flux experiments confirmed that the second transmembrane domains (TM2) of α4 and β2 in 2:3 stoichiometry, $(\alpha4)_2(\beta2)_3$, could form pentameric channels, whereas the α4 TM2 alone could not. The structure, topology, and dynamics of the α4 TM2 and $(\alpha4)_2(\beta2)_3$ TM2 in magnetically aligned phospholipid bicelles were investigated using solid-state NMR spectroscopy in the absence and presence of halothane and isoflurane, two clinically used volatile anesthetics. ^2H NMR demonstrated that anesthetics increased lipid conformational heterogeneity. Such anesthetic effects on lipids became more profound in the presence of transmembrane proteins. PISEMA experiments on the selectively ^{15}N-labeled α4 TM2 showed that the TM2 formed transmembrane helices with tilt angles of $12°\pm1°$ and $16°\pm1°$ relative to the bicelle normal for the α4 and $(\alpha4)_2(\beta2)_3$ samples, respectively. Anesthetics changed the tilt angle of the α4 TM2 from $12°\pm1°$ to $14°\pm1°$, but had only a subtle effect on the tilt angle of the $(\alpha4)_2(\beta2)_3$ TM2. A small degree of wobbling motion of the helix axis occurred in the $(\alpha4)_2(\beta2)_3$ TM2. In addition, a subset of the $(\alpha4)_2(\beta2)_3$ TM2 exhibited counterclockwise rotational motion around the helix axis on a time scale slower than 10^{-4} s in the presence of anesthetics. Both helical tilting and rotational motions have been identified computationally as critical elements for ion channel functions. This study suggested that anesthetics could alter these motions to modulate channel functions.

1. Introduction

Nicotinic acetylcholine receptors (nAChRs) belong to a superfamily of ligand gated ion channels involving the rapid chemical transmission of nerve impulses at synapses. Previous studies found that some subtypes of nAChRs might be potential targets of general anesthetics and their normal channel functions could be inhibited by general anesthetics [1-6]. Neuronal α4β2 nAChR is one of the subtypes sensitive to general anesthetics [4,5,7]. It is also one of the most abundant nAChR subtypes in the brain. Despite ample evidence showing that general anesthetics could alter α4β2 nAChR functions, it remains largely unclear how anesthetics perturb the protein structures and dynamics that ultimately affect the protein functions. Therefore, the insights of anesthetic modulation on the structure and dynamics of the α4β2 nAChR are valuable to resolve a long time mystery of the molecular mechanisms of general anesthesia [8,9].

A comprehensive understanding of anesthetic action on α4β2 nAChR or other nAChR subtypes has often been restricted by limited available structural information of nAChRs in the past. The structural models of the closed- and open-channel α4β2 nAChR have been generated [10] recently via computations using the known structure of the *Torpedo* nAChR as a template [11]. More recent X-ray structures of pentameric ion channels in closed- and open-channel forms from *Erwinia chrysanthemi* and *Gloeobacter violaceus* provide high-resolution structural information relevant to nAChRs [12–14]. These new developments certainly facilitate the understanding of anesthetic action on α4β2 nAChR, but experimental studies of structural and dynamic effects of anesthetics on α4β2 nAChR may lead directly to insights into how anesthetics act on α4β2 nAChR and alter the protein function.

Solid-state NMR spectroscopy is a powerful technique for the characterization of membrane protein structures and dynamics and for the investigation of ligand–protein interactions [15-23]. The polarization Inversion and Spin Exchange at the Magic Angle (PISEMA) experiment [24] is particularly useful for the determination of topological structures and dynamics of helical proteins in a well-oriented lipid environment [25-29]. Ligand binding to the *Torpedo* nAChR was comprehensively analyzed using static ^2H and cross polarization magic angle spinning (CPMAS) ^{13}C solid-state NMR

* Corresponding author. 2049 Biomedical Science Tower 3, 3501 Fifth Avenue, University of Pittsburgh, Pittsburgh, PA 15260. Tel.: +1 412 383 9798; fax: +1 412 648 8998.
E-mail address: tangp@anes.upmc.edu (P. Tang).
[1] Both authors contribute equally to the work.

0005-2736/$ – see front matter © 2009 Elsevier B.V. All rights reserved.
doi:10.1016/j.bbamem.2009.08.009

experiments [30,31]. The structures of the transmembrane domains of the *Torpedo* nAChR were also examined by various solid-state NMR methods [32-34], including PISEMA [33]. However, no solid-state NMR study on neuronal nAChR has been reported previously. In the present study, we embedded the second transmembrane domains (TM2) of α4β2 nAChR in lipid bicelles, which served as membrane mimetic media and magnetically aligned the protein. The structural and dynamic properties of the TM2 α4β2 nAChR in the absence and presence of anesthetics halothane or isoflurane were investigated using solid state NMR, especially PISEMA experiments. Anesthetics were found to affect both helical tilting and rotational motions that have been identified computationally as critical elements for ion channel functions. This study suggested that anesthetics could alter these motions to modulate channel functions.

2. Materials and methods

2.1. Materials and sample preparation

The second transmembrane (TM2) domains of the human nAChR were obtained by solid phase synthesis [35,36]. The α_4 and β_2 TM2 domains have the sequences of EKIT**L**CISV**LL**S**L**TVF**LLL**ITE and EKMTLCISVLLALTVFLLLISK, respectively. In order to simplify the studies, only seven leucine residues in α_4 TM2 domain, as indicated in bold letters, were ^{15}N labeled.

Lipids were purchased from Avanti Polar Lipids (Alabaster, AL). A conventional protocol of bicelle preparation [37] was followed. 1,2-dimyristoyl-sn-glycero-3-phosphocoline (DMPC) and 1,2-dihexyl-sn-glycero-3-phosphocholine (DHPC) were mixed in a desired molar ratio ($q = 3.2$). Lipid concentration was 28% of sample volume (typically 220 μL). To extend sample stability for samples containing the nAChR TM2 domains, 1,2-O-ditetradecyl-sn-glycero-3-phosphocoline (14-O-PC)) and 1,2-O-dihexyl-sn-glycero-3-phosphocholine (6-O-PC) replaced DMPC and DHPC, respectively. A small amount of deuterated $DMPC_{d54}$ (~1 mg) was added to each sample for ^{2}H NMR. The α4 or β2 TM2 was dissolved in 100 μL trifluoroethanol and added to the 6-O-PC-chloroform solution. The organic solvents were removed under a stream of nitrogen gas, followed by further evaporation under high vacuum overnight. The aqueous solutions were prepared by adding 110 μL of deuterium-depleted water to dried 14-O-PC and 6-O-PC/peptide. The 14-O-PC suspension was vortexed extensively followed by three freeze/thaw cycles (liquid nitrogen/42 °C). The 14-O-PC suspension at 42 °C was then added to the 6-O-PC/peptide, followed by vortexing and three freeze/thaw cycles. Slow-speed centrifugation was sometimes necessary to remove air bubbles in the sample. A transparent solution was obtained that was viscous at 38 °C and fluid at 4 °C. Parallel-oriented peptide-containing bicelles were prepared by adding 100 mM $YbCl_3$ $6H_2O$ to the peptide-bicelle solution to reach a final lanthanide concentration of 3 mM. The sample was transferred to a 5-mm OD glass tube (New Era Enterprises, Newfield, NJ) using a pre-cooled pipet tip at 4 °C. The glass tube was sealed with a tight fitting rubber cap and further sealed with hard bees wax. The α4-TM2 concentration was 7.4 mM in the α4 samples and 3 mM in the α4β2 samples. The molar ratio of β2 to α4 was 1.5 in the α4β2 samples to ensure a formation of $(\alpha4)_2(\beta2)_3$. The peptide to lipid ratio is ~1:60. Anesthetics halothane (2-bromo-2-chloro-1,1,1-trifluoro-ethane) and isoflurane (2-chloro-2-(difluoromethoxy)-1,1,1-trifluoro-ethane) were added directly to the NMR tube (pre-cooled in an ice bath) and mixed thoroughly with the samples. The anesthetic concentrations were determined using ^{19}F NMR with 5 mM trifluoroacetic acid (TFA) as a reference.

2.2. NMR spectroscopy

All solid state NMR experiments were performed at 40 °C on a Bruker Avance 600 MHz NMR spectrometer equipped with a ^{1}H/^{31}P/^{15}N(^{2}H) Bruker flat-coil probe. ^{19}F NMR experiments were performed on a Bruker Avance 600 spectrometer with a Bruker TXO probe. The 1-D ^{15}N cross-polarization experiments were conducted using a ^{1}H 90° pulse of 5.1 μs, a 49 kHz ^{1}H-decoupling field, 1 ms contact time, 3 s recycle delay, and 10,000 scans. The same cross-polarization parameters were used in the 2-D ^{15}N-^{1}H PISEMA [38]. Other parameters included ±35 kHz frequency jumps for the Lee-Goldberg condition, 400–1000 scans, and 6–8 s recycle delay. The ^{1}H carrier frequency was set at ~4.5 ppm on parallel oriented bicelle samples. The ^{15}N chemical shift frequencies were referenced to solid ammonium sulfate at 26.8 ppm (relative to liquid ammonia at 0 ppm). The ^{2}H NMR experiments were performed using a solid echo sequence $((\pi/2) - \tau - (\pi/2) - \tau)$. The 90° pulse length was 2 μs and τ values were ~40 μs (perpendicular bicelle) and ~20 μs (parallel bicelle). The recycle delay of 0.5 s and the scans of 256 to 10,000 were used.

2.3. NMR data processing

All NMR spectra were processed using NMRPipe [39] and analyzed using Sparky [40]. The data from PISEMA experiments were fitted to the PISA (Polarity Index Slant Angle) [41,42] wheels using the program developed by Veglia's group [26]. The tilt angle (θ) of the helix axis with respect to the bicelle normal, rotation angle (ρ) of the helix around its axis, the angle between the N-H bond and helix axis (δ), and the dipolar coupling constant (K_{DD}) were determined via fittings. The principal values of the ^{15}N chemical shift tensors [24] for non-glycine residues, $\sigma11 = 64$ ppm, $\sigma22 = 77$ ppm, and $\sigma33 = 217$ ppm, were adopted for the fittings. These values were multiplied uniformly by a factor of 0.95 to accommodate reduced ^{15}N chemical shift anisotropy of proteins in bicelles, as reflected in the reduction of spectral span of the same proteins in bicelles in comparison to those in mechanically aligned lipids.

The TM2 chemical shift assignments were accomplished by combining several sources of information, including the previous assignments of δ–TM2 nAChR [33], the solution NMR structure of β2-TM2 nAChR [36], and the best fitting of PISA wheel. L19 is distinctly separated from the rest of leucine residues in a top view of the NMR structure (pdb code: 2K59) [36]. L19 also has weaker NMR signal than other leucines, presumably because it is located at the lipid-water interface and has less protection from solvent exchange. The distinct location and intensity of L19 convinced us to assign L19 to the most downfield peak in the α4-TM2 PISEMA spectra. Once L19 is defined, the rest of peaks were assigned automatically by PISA wheel fitting. The final assignment of our α4-TM2 PISEMA spectra matches very well with a 2-D projection of the leucine distribution along helical axis from N- to C-terminus in the solution NMR structure [36]. The assignment also agrees well with that for δ–TM2 nAChR [33].

The orientational order parameter, S_i^{CD}, of the ith CD bond vector can relate to the residual quadrupolar splitting, $\Delta\nu^i_Q$, in a ^{2}H NMR spectrum using the equation [43]

$$\Delta\nu_Q^i = \frac{3}{2}A_Q\frac{3\cos^2\theta - 1}{2}S_i^{CD} \quad (1)$$

where $A_Q = e^2Qq/h = 167$ kHz is the static deuterium quadrupolar coupling constant for aliphatic CD bonds, θ is the angle between the bilayer normal and the magnetic field.

2.4. The Na^+ flux assay and confocal fluorescence microscopy

The Na^+ flux assay, as measured by the enhancement of Sodium Green™ dye (Invitrogen, Carlsbad, CA) fluorescence due to Na^+ entry into vesicles through open nAChR channels, is an effective way to assess nAChR activity macroscopically. We prepared 30 mM large lamellar vesicles with 250 μM α4β2. The vesicles contain phosphatidylcholine (PC) and phosphatidylglycerol (PG) in a 4:1 molar ratio

[44]. PC and PG were mixed in chloroform. α4 and β2 were mixed in a molar ratio of 2:3 and dissolved in TFE. The dissolved lipids and α4β2 were mixed and dried to a thin film. Residual organic solvent was removed by vacuum overnight. The lipid–protein mixture was hydrated with a buffer solution at pH 7.5 containing 20 mM Tris, 50 mM $CaCl_2$, and 6uM membrane impermeable Sodium Green™. The vesicles were obtained by incubating the lipid–protein solution at 42 °C overnight and subsequent multiple cycles of freeze and thaw. An extensive dialysis was performed to remove Sodium Green™ dye outside the vesicles.

The Na^+ flux assay was performed using an Olympus Fluoview300 Confocal Laser Scanning head with an Olympus IX70 inverted microscope (Olympus, Melville, NY). Sodium Green™ was excited by the 488-nm argon laser line and the emission was detected using sharp cutoff 510IF long-pass and BA530RIF short-pass filters. For each measurement, 50 μL vesicles containing α4β2 were added into a tray coated with poly-lysine that facilitated vesicle adhesion due to the interactions between negatively charged PG and positively charged poly-lysine. The image acquisition began before the addition of an isotonic 100 mM NaCl solution to the media outside the vesicles and continued for 200 s after the exposure to Na^+. The program MetaMorph was used for analyzing the image data.

3. Results and discussion

3.1. Anesthetic effects on bicelles

Solid-state ^2H NMR spectra of bicelles with deuterated $DMPC_{d54}$, as shown in Fig. 1, provided insight of lipid alignment and dynamics. The high-resolution ^2H NMR spectra with distinguished quadrupolar splittings in Fig. 1A and 1B attested that the bicelles, without incorporating proteins, were well oriented. The quadrupolar splitting of individual ^2H peaks corresponding to carbon positions close to the tail of the aliphatic chains showed little difference in Fig. 1A and 1B, suggesting that anesthetic halothane molecules had no access to the hydrophobic tail region. However, halothane diffused to the carbon positions close to the glycerol group, as evidenced by significantly broadened ^2H signals of the region in Fig. 1B. The order parameters of individual C-^2H bonds of $DMPC_{d54}$, S_{CD}, were calculated using Eq. (1) in the presence and absence of 6 mM halothane. S_{CD} normally contains information on (a) collective motions of lipids, including bicelle wobbling, (b) trans-gauche isomerizations around C-C bonds of lipids, and (c) the anisotropic reorientation of a whole lipid molecule. Collective motions of lipids were small in our systems, in which a 72% hydration level was remained and bicelles were well magnetically oriented. A recent comprehensive NMR analysis also suggested a good bicelle alignment at such a hydration level [45]. The contribution of anisotropic lipid reorientation to S_{CD} was expected to be uniform for all C–^2H bonds linked to a rigid structure. Therefore, a small increase in S_{CD} values in the presence of halothane in Fig. 2 predominately resulted from orientation of the C–^2H bonds with respect to the principal axis of motion of individual lipid molecule. However, since only the readable quadrupolar splitting was used for S_{CD} calculations, the disordered component reflected in the broader peaks might be underestimated in Fig. 2.

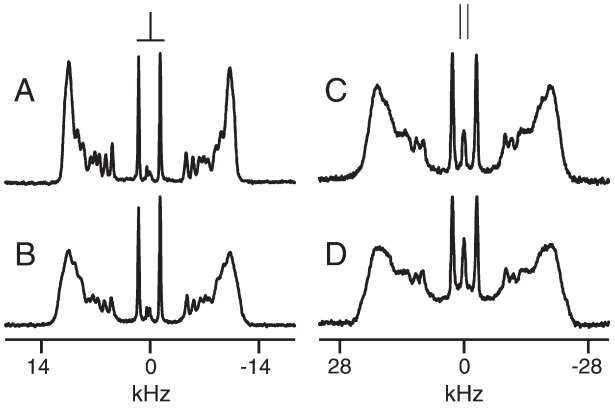

Fig. 1. ^2H NMR spectra of perdeuterated $DPMC_{d54}$ phospholipids embedded in (A) a pure DMPC/DHPC ($q = 3.2$) bicelle system; (B) after adding 6 mM halothane to the system in (A); (C) the 4OPC/6OPC bicelle system incorporated with $(\alpha4)_2(\beta2)_3$ nAChR TM2 domains; (D) after adding 6 mM halothane to the system in (C). The bicelle normal was perpendicular to the magnetic field in (A) and (B), parallel to the magnetic field in (C) and (D) due to the addition of 3 mM lanthanide. The spectra were acquired with the solid echo pulse sequence at 40 °C. The spectrum center was arbitrarily set to 0 Hz.

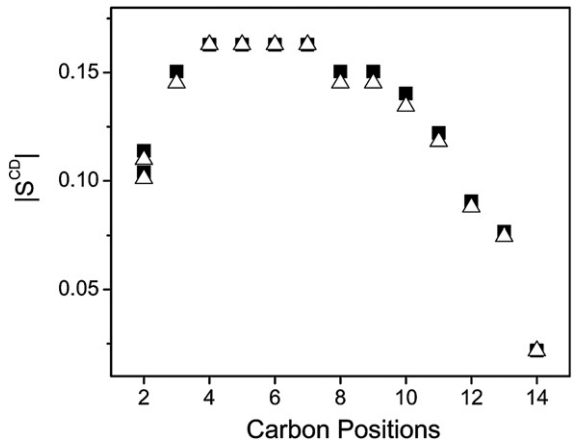

Fig. 2. C-^2H order parameter S_{CD} as a function of $DPMC_{d54}$ carbon positions in the absence (△) and presence (■) of 6 mM anesthetic halothane.

Fig. 1C and D shows the solid-state ^2H NMR spectra of the bicelles incorporated with the $(\alpha4)_2(\beta2)_3$ TM2 in the absence and presence of 6 mM anesthetic isoflurane, respectively. The bicelles were flipped 90° by $YbCl_3$ so that their quadropolar splittings were double of that in Fig. 1A and 1B. The presence of the $(\alpha4)_2(\beta2)_3$ TM2 made the ^2H peaks much broader, presumably because the lipid bilayer was severely disturbed by the insertion of the TM2 domains. A small amount of lipids were in isotropic phase after incorporating TM2 domains into the bicelles and the amount increased upon addition of 6 mM isoflurane, as reflected in the peak at zero frequency. The degree of anesthetics-induced ^2H peak broadening in Fig. 1D seemed to be more severe than that in Fig. 1B, especially to the carbon positions at the middle of DMPC aliphatic chains. Formation of the $(\alpha4)_2(\beta2)_3$ channels might facilitate anesthetic diffusion into the deep bilayer where anesthetics normally have less access. Direct interactions between anesthetics and transmembrane proteins were observed previously [35,46-48]. Anesthetics could modulate protein dynamics directly and allosterically [46]. Such changes in protein motions could affect lipids surrounding proteins and contribute to the observed lipid peak broadening in Fig. 1D.

3.2. TM2 domains in channel and non-channel forms

The α4 and β2 subunits of nAChR need to be in 2:3 stoichiometry to form pentameric channels [49]. Our Na^+ flux experiments confirmed that ion channels could be formed by combining the α4 and β2 TM2 domains in a 2:3 molar ratio, but not by the α4 TM2 domain alone. As shown in Fig. 3, large vesicles made of phosphatidylcholine (PC) and phosphatidylglycerol (PG) with $(\alpha4)_2(\beta2)_3$ TM2 could be easily identified. A time-dependent increase of sodium green fluorescence intensity upon injection of 10 μL 100 mM NaCl signaled channel formation. Control vesicles without channels showed no increase in fluorescence intensity, nor did the channel-containing vesicles when isotonic $CaCl_2$ was added instead of the NaCl solution. The same experiment was also performed on the PC-PG vesicles containing the α4 TM2 domain alone and found no indication of

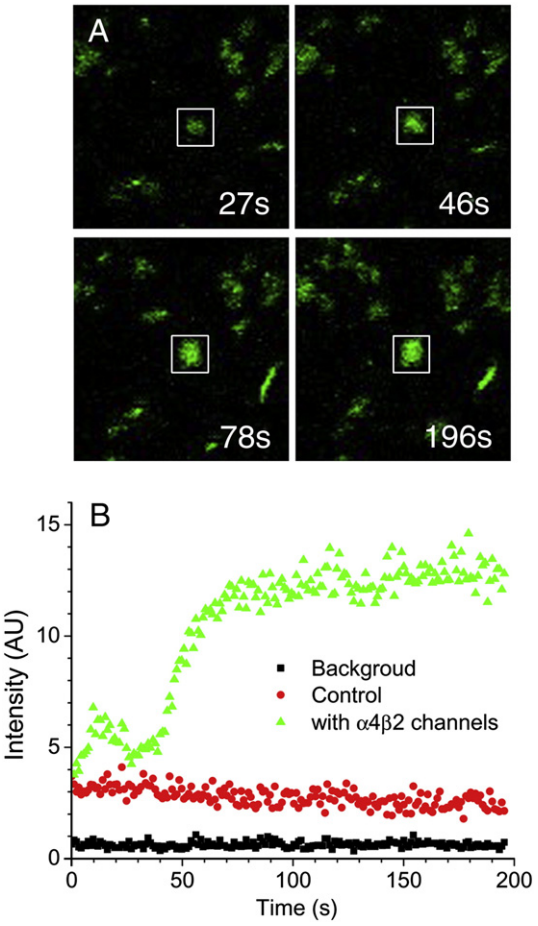

Fig. 3. (A) Confocal fluorescence images of large unilamellar vesicles (LUV) made of phosphatidylcholine and phosphatidylglycerol containing α4β2 nAChR channels after exposure to ~100 mM NaCl solution at different time points. Membrane-impermeable Sodium Green fluorescent dyes were enclosed and trapped inside the LUVs to indicate intra-vesicle Na^+ concentration. The fluorescence intensity of the vesicles with α4β2 channels increased significantly within a short period of time after exposure to extra-vesicle NaCl, indicating an influx of Na^+ through the channels. (B) The intensity changes in the circled vesicles over time after the exposure to extra-vesicle Na^+. The background refers to the region without vesicles. The control refers to vesicles without channels, whose fluorescence intensity remained constant before and after exposure to extra-vesicle Na^+.

channel formation, suggesting different topology and dynamics of the α4 and $(\alpha4)_2(\beta2)_3$ TM2 assemblies.

3.2.1. PISEMA: Effect of β2 TM2 on α4 TM2

The solid state ^1H-^{15}N dipolar /^{15}N chemical shift correlation PISEMA spectra of the ^{15}N-Leu labeled α4 TM2 in Fig. 4 demonstrated distinct differences in the absence and presence of the unlabeled β2 TM2. Wheel-like patterns in the PISEMA spectra of parallel 14-O-PC/6-O-PC bicelles confirmed the transmembrane helical structure of the TM2 domains [36]. Six out of seven total leucine residues of the α4 TM2 showed amide ^{15}N resonances between ~180 and 200 ppm. Their resonance patterns are similar to those composed by the TM2 of the δ nAChR [33]. Leu 5 at the N-terminus of the TM2 did not show up in this region of PISEMA spectra, confirming our early solution NMR finding that Leu 5 was not part of the TM2 helix [36]. Leu 19 resides close to the C terminus of the TM2. Its relatively weak intensity in the PISEMA spectra is probably due to a conformational exchange and less efficient cross-polarization in the dynamic C-terminal region. The most downfield ^{15}N chemical shift in the PISEMA spectra is ~12 ppm smaller than the conventional value of σ33 (217 ppm), suggesting a more dynamical environment in bicelles.

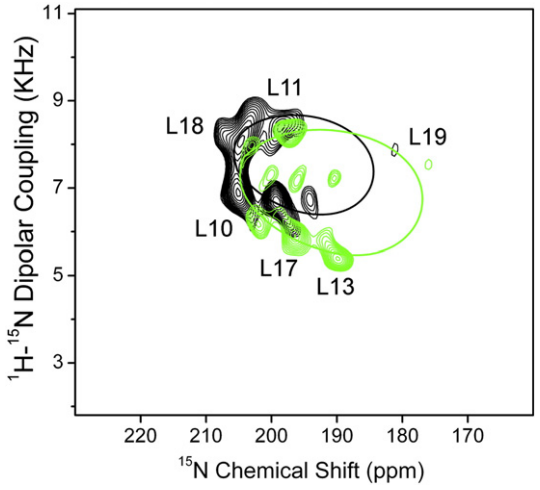

Fig. 4. PISEMA spectra of the ^{15}N-Leu labeled α4 TM2 in the absence (black) and presence (green) of unlabeled β2 TM2. Best fit simulations to the PISEMA data reveal the helical tilt angles of 12 ± 1° and 16 ± 1° of the α4 TM2 and the $(\alpha4)_2(\beta2)_3$ TM2, respectively. The notable difference between two PISEMA spectra suggests that the α4 TM2 must have experienced the existence of the β2 TM2 in the $(\alpha4)_2(\beta2)_3$ TM2 sample.

Although the α4 TM2 had a single set of ^{15}N-Leu resonances in the PISEMA spectrum in Fig. 4, the presence of unlabeled β2 TM2 brought up several minor resonances for the $(\alpha4)_2(\beta2)_3$ TM2. Leu10, Leu17, and Leu13 showed almost the same ^{15}N chemical shifts in both major and minor resonances, but their dipolar couplings were about 1 kHz greater in the minor resonances. Although it was almost impossible to accurately define topology of the minor conformation due to too few numbers of resonances, the chemical shift and dipolar coupling data suggested that the helix tilt angle relative to the bicelle normal must be smaller in the minor conformation than in the major population [41,42]. The minor peaks might also result from a sub-population α4 TM2 in a slightly different motional environment.

A more noticeable difference between the α4 and $(\alpha4)_2(\beta2)_3$ spectra in Fig. 4 is the shift of the amide resonances along both ^{15}N chemical shift and ^1H-^{15}N dipolar coupling axis. Leu11 and Leu18 of the α4 TM2 experienced relatively small shifts before and after mixing with the β2 TM2, but Leu10, Leu13, Leu17 and Leu19 had more profound changes. It is plausible that Leu11 and Leu18 have experienced little interaction with residues in other helices. The best fitting of all downfield resonances to ideal PISA wheels revealed the helical tilt angles of 12 ± 1° and 16 ± 1° of the α4 TM2 and the $(\alpha4)_2(\beta2)_3$ TM2, respectively. The rotation angle, ρ, was 65° for both α4 and $(\alpha4)_2(\beta2)_3$. The tilt angle of 12° for the α4 TM2 in bicelles agrees with the result of the δ nAChR [33], where the δ TM2 helix was also tilted 12° relative to the normal of mechanically oriented DMPC bilayers. Neither α4 nor δ subunit could form nAChR channels without partitioning of other subunit types [49]. The tilt angle of 16 ± 1° of the $(\alpha4)_2(\beta2)_3$ TM2 is comparable to the tilt angle of 15 ± 2° found for the $GABA_A$ receptor TM2 domain, an anion channel-forming peptide, by a recent solid-state NMR study [18].

It is worth mentioning that all the resonances in our PISEMA spectra resulted solely from the ^{15}N-Leu residues of the α4 TM2. The unlabeled β2 TM2 did not generate ^{15}N NMR signals. If the α4 TM2 was isolated from the β2 TM2, the $(\alpha4)_2(\beta2)_3$ TM2 would give the same PISEMA spectrum as the α4 TM2. The notable difference between the two spectra in Fig. 4 prove that the α4 TM2 must have interacted with the β2 TM2 in the $(\alpha4)_2(\beta2)_3$ TM2 sample. A thorough NMR characterization of oligomerization states of ^2H selective labeled transmembrane peptides in oriented lipid bilayers was demonstrated previously [50]. The same method can also be applied to the α4 and β2 TM2 if proper labeled samples become available. Nevertheless, the data in Fig. 4 indicate that interaction

between α4 and β2 subunits that might be the driving force for assembling a functional channel. The larger helix tilt angle found in the $(\alpha4)_2(\beta2)_3$ TM2 supported the previous prediction that channel opening might involve tilting of pore lining helices [10,12,51,52].

3.3. Anesthetic effect on the TM2 domains

Fig. 5 displays an overlay of the PISEMA spectra of the α4 TM2 in the absence and presence of 6 mM halothane. Halothane lowered ^{1}H-^{15}N dipolar coupling and ^{15}N chemical shift of six leucine residues noticeably. The data fitting into PISA wheels provided a helical tilt angle of 14° in the presence of halothane. The dipolar coupling constant, K_{DD}, decreased from 8700 to 8100 KHz, but the rotational angle ($\rho = 65°$) and the angle between N-H bone and helix axis ($\delta = 13°$) remained the same in the absence and presence of 6 mM halothane.

In comparison to the α4 TM2, the $(\alpha4)_2(\beta2)_3$ TM2 seemed less susceptible to anesthetics. Fig. 6 shows the PISEMA spectra of the $(\alpha4)_2(\beta2)_3$ TM2 before and after adding 12 mM anesthetic isoflurane. The helix tilt angle of the $(\alpha4)_2(\beta2)_3$ TM2 with respect to the bicelle normal changed less than 1° ($\theta = 16.5°$). The K_{DD} value changed from 8400 to 7900 KHz. The other two parameters, $\rho = 65°$ and $\delta = 13°$, remain unchanged. To the majority of the $(\alpha4)_2(\beta2)_3$ TM2 in the sample, anesthetic isoflurane had a subtle but real impact on their helical orientation in bicelles. The anesthetic-induced changes in the major resonance pattern also implicate the possibility of a wobbling motion of the helix axis with respect to the bicelle normal [53]. Those aforementioned minor resonances of Leu10, Leu13, and Leu17 shown in Fig. 4 disappeared after adding 6 mM isoflurane to the sample (see the on-line supporting information). However, another subset of minor resonances appeared upon further increasing the isoflurane concentration to 12 mM, as shown in Fig. 6. The new minor peaks, labeled as L19′, L11′, L13′ L17′, and L19′ in Fig. 6, appeared as if they resulted from corresponding major resonances rotating ~50° counterclockwise around the helical axis. Distinct major and minor resonances signify that the helix rotational motion was on a time scale slower than 10^{-4} s [54]. Both tilting and rotational motions of the TM2 helices are critical elements for channel functions [10]. Our data reveal that anesthetic molecules are able to alter motions of the TM2 helices that could account, at least partially, for anesthetic inhibition effects on the α4β2 nAChR [7].

It is not surprising to observe different responses of the α4 TM2 and the $(\alpha4)_2(\beta2)_3$ to anesthetics, considering that one might exist as monomer but the other could form channels. Without the presence of

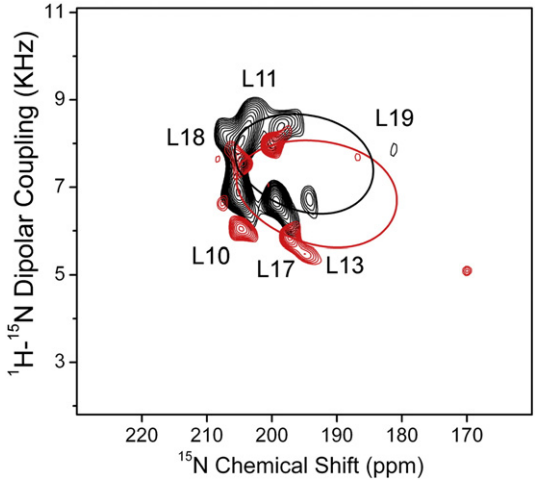

Fig. 5. An overlay of PISEMA spectra of the α4 TM2 in the absence (black) and presence (red) of 6 mM halothane. PISA wheel fitting of the α4 TM2 in the presence of 6 mM halothane reveals an increase in tilt angle from 12° ± 1° to 14° ± 1°.

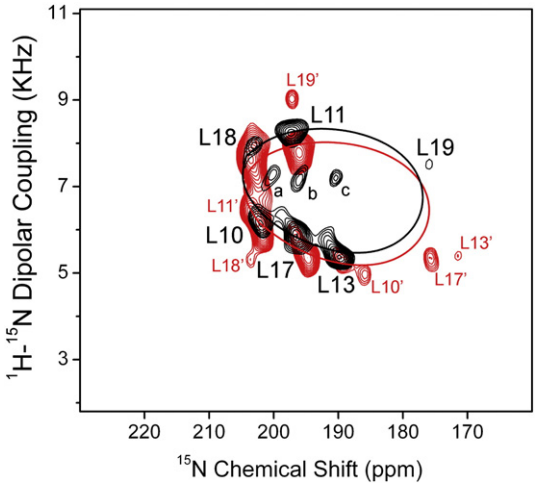

Fig. 6. An overlay of PISEMA spectra of the $(\alpha4)_2(\beta2)_3$ TM2 in the absence (black) and presence (red) of 12 mM anesthetic isoflurane. Notice the appearance of subset resonance peaks (a, b, c in black and L19′, L11′, L18′, L19′, L13′, L17′ in red). The minor resonance peaks in red seem to result from rotating corresponding major resonances ~50° counterclockwise around the helical axis.

the β2 TM2, the α4 TM2 interacted loosely with other α4 TM2 helices so that individual helix orientation was affected by anesthetics more severely. In a pentameric $(\alpha4)_2(\beta2)_3$ TM2, the helix tilting in respect to the bicelle normal became less sensitive to the addition of anesthetics, presumably due to stronger interaction between the α4 TM2 and its adjacent β2 TM2. One may wonder if small changes in helix orientation induced by anesthetics, either through tilting or rotational motion, are significant enough to alter channel functions. The X-ray structures of pentameric ion channels from bacterial demonstrated that the pore-lining TM2 domains in closed- and open-channel conformations differ by merely 9° rotation around an axis that is parallel to the membrane normal [12-14], suggesting that a small change in the TM2 orientation could elicit a sizable change in channel functions. Although further structural and dynamical investigations on integral α4β2 nAChR are necessary to define a final answer, the present study highlights the possibility that anesthetics may modulate the channel function via altering the motion as well as orientation of the pore-ling domain.

4. Conclusions

Several key findings emerged from the current study. First, transmembrane proteins could facilitate anesthetic diffusion into deep membrane bilayers even though anesthetics normally prefer amphiphilic lipid-water interface region [55]. Consequently, anesthetics affected lipid alignment and conformation more severely in bicelles containing proteins. Secondly, the α4 TM2 could not form channels unless it had been mixed with the β2 TM2. The interactions between the α4 and β2 TM2 subunits do exist and such interactions may be essential to drive channel formation. Thirdly, general anesthetics could perturb orientations of the transmembrane helices in lipid bilayers and introduce changes in helical motions. The observed anesthetic effects on the tilt and rotational angles of pore lining TM2 helices reveal a potential pathway for anesthetic inhibition of channel functions. A more challenging question has arisen based on the current study: how do anesthetics make changes in transmembrane protein orientations and motions that are related to protein functions? This is certainly a question worth further investigation.

Acknowledgements

The authors thank Dr. Yuanyuan Jia for her contribution to sample preparations and initial experiment set up, Dr. Jochem Struppe of

Bruker for his suggestions in setting up the PISEMA experiment, Dr. Christopher V. Grant of UCSD for his suggestions in initial sample preparation and selection of parameters for experiments and data process, Prof. Gianluigi Veglia and Dr. Nate Traaseth of University of Minnesota and Prof. Timothy A. Cross and Dr. Conggang Li of Florida State University for sharing their PISA wheel simulation programs with us. This work was supported in part by grants from the National Institute of Health (R01GM56257 and R01GM66358 to P.T. and R37GM049202 to Y.X.).

Appendix A. Supplementary data

Supplementary data associated with this article can be found, in the online version, at doi:10.1016/j.bbamem.2009.08.009.

References

[1] S.A. Forman, K.W. Miller, G. Yellen, A discrete site for general anesthetics on a postsynaptic receptor, Mol. Pharmacol. 48 (1995) 574–581.
[2] R.A. Cardoso, S.J. Brozowski, L.E. Chavez-Noriega, M. Harpold, C.F. Valenzuela, R.A. Harris, Effects of ethanol on recombinant human neuronal nicotinic acetylcholine receptors expressed in Xenopus oocytes, J. Pharmacol. Exp. Ther. 289 (1999) 774–780.
[3] D.E. Raines, V.T. Zachariah, Isoflurane increases the apparent agonist affinity of the nicotinic acetylcholine receptor [see comments], Anesthesiology 90 (1999) 135–146.
[4] T. Mori, X. Zhao, Y. Zuo, G.L. Aistrup, K. Nishikawa, W. Marszalec, J.Z. Yeh, T. Narahashi, Modulation of neuronal nicotinic acetylcholine receptors by halothane in rat cortical neurons, Mol. Pharmacol. 59 (2001) 732–743.
[5] M. Yamashita, T. Mori, K. Nagata, J.Z. Yeh, T. Narahashi, Isoflurane modulation of neuronal nicotinic acetylcholine receptors expressed in human embryonic kidney cells, Anesthesiology 102 (2005) 76–84.
[6] E. Arevalo, D.C. Chiara, S.A. Forman, J.B. Cohen, K.W. Miller, Gating-enhanced accessibility of hydrophobic sites within the transmembrane region of the nicotinic acetylcholine receptor's {delta}-subunit. A time-resolved photolabeling study, J. Biol. Chem. 280 (2005) 13631–13640.
[7] P. Flood, J. Ramirez-Latorre, L. Role, Alpha 4 beta 2 neuronal nicotinic acetylcholine receptors in the central nervous system are inhibited by isoflurane and propofol, but alpha 7-type nicotinic acetylcholine receptors are unaffected, Anesthesiology 86 (1997) 859–865.
[8] N.P. Franks, W.R. Lieb, Do general anaesthetics act by competitive binding to specific receptors? Nature 310 (1984) 599–601.
[9] J.A. Campagna, K.W. Miller, S.A. Forman, Mechanisms of actions of inhaled anesthetics, N. Engl. J. Med. 348 (2003) 2110–2124.
[10] E.J. Haddadian, M.H. Cheng, R.D. Coalson, Y. Xu, P. Tang, In Silico Models for the Human alpha4beta2 Nicotinic Acetylcholine Receptor, J. Phys. Chem. B. 112 (2008) 13981–13990.
[11] N. Unwin, Refined structure of the nicotinic acetylcholine receptor at 4 Å resolution, J. Mol. Biol. 346 (2005) 967–989.
[12] R.J. Hilf, R. Dutzler, X-ray structure of a prokaryotic pentameric ligand-gated ion channel, Nature 452 (2008) 375–379.
[13] R.J. Hilf, R. Dutzler, Structure of a potentially open state of a proton-activated pentameric ligand-gated ion channel, Nature 457 (2009) 115–118.
[14] N. Bocquet, H. Nury, M. Baaden, C. Le Poupon, J.P. Changeux, M. Delarue, P.J. Corringer, X-ray structure of a pentameric ligand-gated ion channel in an apparently open conformation, Nature 457 (2009) 111–114.
[15] N.J. Traaseth, L. Shi, R. Verardi, D.G. Mullen, G. Barany, G. Veglia, Structure and topology of monomeric phospholamban in lipid membranes determined by a hybrid solution and solid-state NMR approach, Proc. Natl. Acad. Sci. U. S. A. 106 (2009) 10165–10170.
[16] V.S. Bajaj, M.L. Mak-Jurkauskas, M. Belenky, J. Herzfeld, R.G. Griffin, Functional and shunt states of bacteriorhodopsin resolved by 250 GHz dynamic nuclear polarization-enhanced solid-state NMR, Proc. Natl. Acad. Sci. U. S. A. 106 (2009) 9244–9249.
[17] E. Salnikov, C. Aisenbrey, V. Vidovic, B. Bechinger, Solid-state NMR approaches to measure topological equilibria and dynamics of membrane polypeptides, Biochim. Biophys. Acta (2009).
[18] S.K. Kandasamy, D.K. Lee, R.P. Nanga, J. Xu, J.S. Santos, R.G. Larson, A. Ramamoorthy, Solid-state NMR and molecular dynamics simulations reveal the oligomeric ion-channels of TM2-GABA(A) stabilized by intermolecular hydrogen bonding, Biochim. Biophys. Acta 1788 (2009) 686–695.
[19] A. McDermott, Structure and dynamics of membrane proteins by magic angle spinning solid-state NMR, Annu. Rev. Biophys. 38 (2009) 385–403.
[20] C. Li, M. Yi, J. Hu, H.X. Zhou, T.A. Cross, Solid-state NMR and MD simulations of the antiviral drug amantadine solubilized in DMPC bilayers, Biophys. J. 94 (2008) 1295–1302.
[21] S.J. Opella, A.C. Zeri, S.H. Park, Structure, dynamics, and assembly of filamentous bacteriophages by nuclear magnetic resonance spectroscopy, Annu. Rev. Phys. Chem. 59 (2008) 635–657.
[22] M. Hong, Structure, topology, and dynamics of membrane peptides and proteins from solid-state NMR spectroscopy, J. Phys. Chem. B. 111 (2007) 10340–10351.
[23] A. Watts, Solid-state NMR in drug design and discovery for membrane-embedded targets, Nat. Rev. Drug Discov. 4 (2005) 555–568.
[24] C.H. Wu, A. Ramamoorthy, L.M. Gierasch, S.J. Opella, Simultaneous Characterization of the Amide 1H Chemical Shift, 1H-15N Dipolar, and 15N Chemical Shift Interaction Tensors in a Peptide Bond by Three-Dimensional Solid-State NMR Spectroscopy, J. Am. Chem. Soc. 117 (1995) 6148–6149.
[25] R. Fu, M. Truong, R.J. Saager, M. Cotten, T.A. Cross, High-resolution heteronuclear correlation spectroscopy in solid state NMR of aligned samples, J. Magn. Reson. 188 (2007) 41–48.
[26] J.J. Buffy, N.J. Traaseth, A. Mascioni, P.L. Gor'kov, E.Y. Chekmenev, W.W. Brey, G. Veglia, Two-dimensional solid-state NMR reveals two topologies of sarcolipin in oriented lipid bilayers, Biochemistry 45 (2006) 10939–10946.
[27] C. Li, P. Gao, H. Qin, R. Chase, P.L. Gor'kov, W.W. Brey, T.A. Cross, Uniformly aligned full-length membrane proteins in liquid crystalline bilayers for structural characterization, J. Am. Chem. Soc. 129 (2007) 5304–5305.
[28] U.H. Durr, L. Waskell, A. Ramamoorthy, The cytochromes P450 and b5 and their reductases–promising targets for structural studies by advanced solid-state NMR spectroscopy, Biochim. Biophys. Acta 1768 (2007) 3235–3259.
[29] A.W. Ramamoorthy, Y. Lee, D.K., PISEMA solid-state NMR spectroscopy, Ann. Rep. NMR Spectrosc. 52 (2004) 1–52.
[30] P.T. Williamson, A. Verhoeven, K.W. Miller, B.H. Meier, A. Watts, The conformation of acetylcholine at its target site in the membrane-embedded nicotinic acetylcholine receptor, Proc. Natl. Acad. Sci. U. S. A. 104 (2007) 18031–18036.
[31] P.T. Williamson, B.H. Meier, A. Watts, Structural and functional studies of the nicotinic acetylcholine receptor by solid-state NMR, Eur. Biophys. J. 33 (2004) 247–254.
[32] M.R. de Planque, D.T. Rijkers, J.I. Fletcher, R.M. Liskamp, F. Separovic, The alphaM1 segment of the nicotinic acetylcholine receptor exhibits conformational flexibility in a membrane environment, Biochim. Biophys. Acta 1665 (2004) 40–47.
[33] S.J. Opella, F.M. Marassi, J.J. Gesell, A.P. Valente, Y. Kim, M. Oblatt-Montal, M. Montal, Structures of the M2 channel-lining segments from nicotinic acetylcholine and NMDA receptors by NMR spectroscopy, Nat. Struct. Biol. 6 (1999) 374–379.
[34] P.T. Williamson, G. Zandomeneghi, F.J. Barrantes, A. Watts, B.H. Meier, Structural and dynamic studies of the gamma-M4 trans-membrane domain of the nicotinic acetylcholine receptor, Mol. Membr. Biol. 22 (2005) 485–496.
[35] V. Bondarenko, V.E. Yushmanov, Y. Xu, P. Tang, NMR study of general anesthetic interaction with nAChR beta2 subunit, Biophys. J. 94 (2008) 1681–1688.
[36] V.E. Yushmanov, Y. Xu, P. Tang, NMR structure and dynamics of the second transmembrane domain of the neuronal acetylcholine receptor beta 2 subunit, Biochemistry 42 (2003) 13058–13065.
[37] A.A. De Angelis, S.C. Howell, A.A. Nevzorov, S.J. Opella, Structure determination of a membrane protein with two trans-membrane helices in aligned phospholipid bicelles by solid-state NMR spectroscopy, J. Am. Chem. Soc. 128 (2006) 12256–12267.
[38] C.H. Wu, A. Ramamoorthy, S.J. Opella, High-Resolution Heteronuclear Dipolar Solid-State NMR Spectroscopy, J. Magn. Reson., Ser. A 109 (1994) 270–272.
[39] F. Delaglio, S. Grzesiek, G.W. Vuister, G. Zhu, J. Pfeifer, A. Bax, NMRPipe: a multidimensional spectral processing system based on UNIX pipes, J. Biomol. NMR 6 (1995) 277–293.
[40] T.D. Goddard, and Kneller, D.G, University of California, San Francisco.
[41] J. Wang, J. Denny, C. Tian, S. Kim, Y. Mo, F. Kovacs, Z. Song, K. Nishimura, Z. Gan, R. Fu, J.R. Quine, T.A. Cross, Imaging membrane protein helical wheels, J. Magn. Reson. 144 (2000) 162–167.
[42] F.M. Marassi, S.J. Opella, A solid-state NMR index of helical membrane protein structure and topology, J. Magn. Reson. 144 (2000) 150–155.
[43] J.H. Davis, The description of membrane lipid conformation, order and dynamics by 2H-NMR, Biochim. Biophys. Acta 737 (1983) 117–171.
[44] P. Tang, J. Hu, S. Liachenko, Y. Xu, Distinctly different interactions of anesthetic and nonimmobilizer with transmembrane channel peptides, Biophys. J. 77 (1999) 739–746.
[45] K. Yamamoto, R. Soong, A. Ramamoorthy, Comprehensive analysis of lipid dynamics variation with lipid composition and hydration of bicelles using nuclear magnetic resonance (NMR) spectroscopy, Langmuir 25 (2009) 7010–7018.
[46] C.G. Canlas, T. Cui, L. Li, Y. Xu, P. Tang, Anesthetic modulation of protein dynamics: insights from a NMR study, J. Phys. Chem. B. 112 (2008) 14312–14318.
[47] Y. Xu, T. Seto, P. Tang, L. Firestone, NMR study of volatile anesthetic binding to nicotinic acetylcholine receptors, Biophys. J. 78 (2000) 746–751.
[48] Y. Xu, P. Tang, Amphiphilic sites for general anesthetic action? Evidence from 129Xe-[1H] intermolecular nuclear Overhauser effects, Biochim. Biophys. Acta 1323 (1997) 154–162.
[49] D.S. McGehee, Molecular diversity of neuronal nicotinic acetylcholine receptors, Ann. N. Y. Acad Sci. 868 (1999) 565–577.
[50] C. Aisenbrey, B. Bechinger, Investigations of polypeptide rotational diffusion in aligned membranes by 2H and 15 N solid-state NMR spectroscopy, J. Am. Chem. Soc. 126 (2004) 16676–16683.
[51] P. Tang, P.K. Mandal, Y. Xu, NMR structures of the second transmembrane domain of the human glycine receptor alpha(1) subunit: model of pore architecture and channel gating, Biophys. J. 83 (2002) 252–262.
[52] A. Szarecka, Y. Xu, P. Tang, Dynamics of heteropentameric nicotinic acetylcholine receptor: implications of the gating mechanism, Proteins 68 (2007) 948–960.
[53] R.C. Page, S. Kim, T.A. Cross, Transmembrane helix uniformity examined by spectral mapping of torsion angles, Structure 16 (2008) 787–797.
[54] A. Abragam, Principles of Nuclear Magnetism, 315, Oxford University Press, New York, 1961.
[55] P. Tang, B. Yan, Y. Xu, Different distribution of fluorinated anesthetics and nonanesthetics in model membrane: a 19F NMR study, Biophys. J. 72 (1997) 1676–1682.